Article:
Gonzalez-Carter, DA, Ong, ZY orcid.org/0000-0001-8666-4382, McGilvery, CM et al. (3 more authors) (2019) L-DOPA functionalized, multi-branched gold nanoparticles as brain-targeted nano-vehicles. Nanomedicine: Nanotechnology, Biology and Medicine, 15 (1). pp. 1-11. ISSN 1549-9634

https://doi.org/10.1016/j.nano.2018.08.011

L-DOPA Functionalized, Multi-Branched Gold Nanoparticles as Brain-targeted Nano-Vehicles

Daniel Gonzalez-Carter[a,b,#,§,*], Zhan Yuin Ong[c,d, §,*], Catriona M. McGilvery[a], Iain E. Dunlop[a], David T. Dexter[b], Alexandra E. Porter[a]

[a]Department of Materials, Imperial College London, Exhibition Road, London, U.K. SW7 2AZ

[b]Centre for Neuroinflammation and Neurodegeneration, Division of Brain Sciences, Imperial College London, Hammersmith Hospital Campus, London, U.K. W12 0NN

[c]School of Physics and Astronomy, and [d] Leeds Institute of Biomedical and Clinical Sciences, School of Medicine, University of Leeds, Leeds, U.K. LS2 9JT

[#]Current address: Innovation Center of NanoMedicine, 3 Chome-25-14, Tonomachi, Kawasaki, Japan. 210-0821

[*]Corresponding authors: carter-d@kawasaki-net.ne.jp (+81-(0)-44-589-5700), z.y.ong@leeds.ac.uk (+44-(0)-113-343-0051)
[§]These authors contributed equally.

Abstract word count: 150; manuscript word count: 4,960; References: 38; Number of figures/tables: 5

Abstract

The blood-brain barrier (BBB) is a protective entholelial barrier lining the brain microvasculature which prevents brain delivery of the majority of therapies against brain diseases. Hence, there is an urgent need to develop vehicles which efficiently penetrate the BBB to deliver therapies into the brain. The drug L-DOPA efficiently and specifically crosses the BBB *via* the large amino acid transporter (LAT)-1 protein to enter the brain. Thus, we synthesized L-DOPA-functionalized multi-branched nanoflower-like gold nanoparticles (L-DOPA-AuNF) using a seed-mediated method involving catechols as a direct reducing-cum-capping agent, and examined their ability to cross the BBB to act as brain-penetrating nano-vehicles. We show L-DOPA-AuNF efficiently penetrate the BBB compared to similarly sized and shaped AuNFs functionalized with a non-targeting ligand. Furthermore, we show L-DOPA-AuNF are efficiently internalized by brain macrophages without inducing inflammation. These results demonstrate the application of L-DOPA-AuNF as a non-inflammatory brain-specific nano-vehicle to efficiently deliver therapies into the brain.

Key words: Brain targeting, blood-brain barrier, gold nanoparticles, L-DOPA

Funding Z.Y.O.: People Programme (Marie Curie Actions) of the European Union's Seventh Framework Programme FP7-PEOPLE-2013-IIF under REA grant agreement no.[624475]; University of Leeds Academic Fellowship. A.E.P.: ERC starting grant (CNTBBB); Michael J. Fox Foundation grant (#11713); Elsie Widdowson Fellowship.

Background

Development of therapies and diagnostics (theranostics) against brain disorders such as Parkinson's disease (PD) is hampered by the inability of macromolecules to enter the brain due to the protective blood-brain barrier (BBB)[1], a highly impermeable endothelial layer lining the brain microvasculature. Hence, the successful development of vehicles capable of penetrating the BBB will significantly increase the number of clinically viable theranostics to combat brain diseases.

Gold nanoparticles (AuNP) are an attractive platform to deliver theranostics into the brain as they are highly biocompatible and their surfaces are easily modified with various functional groups, allowing for a wide range of brain-targeting and cargo-delivery strategies to be employed[2]. Furthermore, AuNP can be imaged *in vivo* using non-invasive X-ray computed tomography (CT)[3], without the need for additional chemical labelling procedures.

Although AuNP functionalised with transferrin[4,5] glucose[6], and insulin[7] have demonstrated BBB penetration, lack of brain specificity remains an issue which may lead to unwanted side-effects in peripheral organs. Hence, a more specific targeting ligand is required to resolve such inadequacies for effective clinical translation.

Functionalizing AuNP with the drug L-DOPA is an attractive, yet unexploited, strategy for specific brain delivery. L-DOPA is an FDA-approved drug employed in the clinic against PD which is actively transported across the BBB by the large neutral amino acid transporter-1 (LAT-1) into the brain to replace dopamine. Hence, its ability to penetrate the BBB in an efficient, safe and non-toxic manner is well established. Importantly, LAT-1 is highly expressed at the BBB compared to peripheral non-barrier tissues[8], enabling enhanced brain penetration. Furthermore, the binding affinity of L-DOPA to LAT-1 is relatively high (K_m 150-200 μM)[9], allowing L-DOPA/LAT-1 interaction to occur even for nanoparticles with low ligand densities, resulting in high levels of nanoparticle capture.

Previously, we have demonstrated the use of catechols including L-DOPA, D-DOPA, dopamine, and 4-ethylcatechol as efficient reducing-cum-capping agents for the seed mediated synthesis of monodisperse nanoflower-like gold nanoparticles (AuNF) to target breast cancer cells[10]. The catechol

functional group of L-DOPA efficiently reduces Au^{3+} to Au^{0} on the surface of gold seeds and eventually adsorbs on the surface of the AuNFs to present the primary α-amino and α-carboxyl groups necessary for interaction with LAT-1. As such, this synthetic procedure affords a simple and cost-effective means of obtaining multi-branched, catechol-functionalized AuNF without the need for lengthy and costly conjugations with targeting peptides, antibodies, or aptamers. Additionally, multi-branched AuNFs are a more attractive brain-penetrating nano-vehicle platform than spherical AuNPs as they have a larger surface area available for drug loading and can be easily tuned to absorb near infrared (NIR) light for photothermal therapy and bioimaging[10].

In the present study, we expanded our previous work to examine whether multi-branched AuNF functionalized with the LAT-1-targeting ligands L-DOPA or its chiral isomer D-DOPA, which is recognized by LAT-1 along with other D-isomer amino-acids [11-13], safely and efficiently penetrate the BBB compared to similarly shaped and sized AuNFs functionalized with non-targeting control ligands (4-ethyl catechol or dopamine) in order to lay the foundations for the application of L-DOPA-functionalized AuNF as a brain-specific nano-vehicle for brain imaging and theranostics delivery in the clinic. The ability of AuNF to enter the brain was examined on an *in vitro* model of the human BBB employing the immortalized human brain endothelial cell line hCMEC/D3[14] and validated using primary brain endothelial monolayers isolated from adult rat brains. In addition, AuNF uptake by brain macrophages (microglia cells) was characterized to examine AuNF clearance and inflammation induction following brain penetration to further establish their safe application as vehicles for theranostics against brain diseases.

Methods

Unless otherwise stated, all materials were supplied by Sigma-Aldrich (U.K.).

AuNF synthesis and characterization

Synthesis: AuNF were synthesized using a seed-mediated method as previously described[10]. Briefly, spherical gold seeds (14 nm) were prepared by reducing gold chloride with sodium citrate using the

Turkevich method. To obtain L-DOPA-functionalized AuNF, 100μL of 0.1M $HAuCl_4 \cdot 3H_2O$ and 400μL of 10mg/mL of mPEG thiol were added to an aqueous dispersion of spherical gold seeds, followed by the addition of 4.0mL of 15mM L-DOPA solution under vigorous stirring at room temperature (RT). The synthesized AuNF were purified by centrifugation and rinsing with Milli-Q water to obtain a dark-blue colloidal dispersion. AuNF were functionalized with the LAT-1 targeting ligands L-DOPA (L-DOPA-AuNF) or D-DOPA (D-DOPA-AuNF). Non-targeting controls with similar size, morphology and ζ-potential were prepared by functionalizing AuNF with 4-ethylcatechol (4-EC-AuNF) or dopamine (DA-AuNF), as described in our previous publication[10]. Both 4-EC and DA lack the necessary amino-carboxyl moiety required for LAT-1 recognition[15].

Characterization: Full characterization of the synthesized AuNFs has been described in our previous publication[10]. Briefly, AuNFs were characterized by bright-field high-resolution transmission electron microscopy (TEM) using a JEOL JEM-2100F operated at 200kV, and UV-vis-NIR spectrophotometry (Agilent Cary 6000i). Hydrodynamic diameter and zeta-potential were characterized through dynamic light scattering (DLS) employing a Zetasizer Nano (Malvern Instrument Ltd). Elemental gold concentration of AuNF was determined using inductively coupled plasma-atomic emission spectroscopy (ICP-AES; ThermoScientific iCAP 6300 Duo). The successful surface functionalization of the AuNF with catechols was confirmed using X-ray photoelectron spectrophotometry (XPS; Thermo Scientific K-Alpha$^+$ X-ray Photoelectron Spectrophotometer).

Cell culture

Human brain endothelial cells: The immortalized human brain endothelial cell line hCMEC/D3 was obtained from Dr. Romero, Open University, U.K. hCMEC/D3 were established by lentiviral vector transduction of endothelial cells derived from human temporal lobe microvessels with human telomerase (hTERT) and SV40 large T antigen[16]. hCMEC/D3 form tight, polarized monolayers with low paracellular flux and expression of transporters closely mimicking the *in vivo* condition[17-19]. hCMEC/D3 were cultured in Cell-Bind culture flasks (Corning, UK) in EBM-2 medium (Lonza, Switzerland) supplemented with vascular endothelial growth factor (VEGF) (unless otherwise stated), insulin-like growth factor-1 (IGF1), epidermal growth factor (EGF), basic fibroblast growth factor

(bFGF), hydrocortisone, ascorbic acid, gentamycin, and 2.5% (v/v) foetal calf serum (FCS) (hereafter termed full EBM). Cells were incubated at 37ºC in 5% CO_2, and passaged by detachment with trypsin/EDTA. Cells were employed between passages 25-35.

Primary rat brain microvascular endothelial cells (1ºEC): All procedures were carried out in accordance with the Animals (Scientific Procedures) Act, 1986. Brain microvascular endothelial cells were extracted from adult male Wistar rats (150g, Charles River, UK) employing a BSA-density centrifugation isolation method[20]. Briefly, rats were sacrificed (CO_2 exposure and cervical dislocation) and the brain cortex isolated over ice-cold dissection buffer (HBSS with 1%BSA and 2% penicillin/streptomycin). Following removal of the sub-cortical myelin, meninges and all visible blood vessels, the brains were homogenized in ice-cold dissection buffer followed by incubation in digestion buffer (DMEM/Ham's F12 with collagenase, dispase, DNase type I and trypsin) at 37ºC. The brain digest solution was mixed with separation gradient buffer (25% BSA) and centrifuged. The microvessel pellet was incubated in digestion buffer (1hr at 37ºC), followed by centrifugation and plating in culturing medium (full EBM with 4µg/mL puromycin and 100µg/mL endothelial cell growth supplement) employing Cell-BIND T75 cell culture flasks (Corning, USA) coated with calf skin collagen type-I (100µg/mL) and bovine plasma fibronectin (10µg/mL). After 5 days, the culture medium was changed to low puromycin (1µg/mL) until reaching confluency. The brain endothelial cells were then trypsinized (trypsin/EDTA) and aliquoted in freezing medium (DMEM with 10 % FCS, 10% DMSO) to create frozen stocks. For experiments, cells were defrosted, expanded in full EBM as above and plated in appropriate plastic-ware. Isolated primary rat brain endothelial cells formed a highly pure, homogenous monolayer with minimal intercellular gaps as evidenced by even cellular distribution with extensive cell-to-cell contact, formation of alignment patterns and lack of contaminating cells (fig. S1a). In addition, the monolayers adopted a BBB phenotype, as demonstrated by intercellular expression of the tight-junction proteins zona occludens-1 (fig. S1b) and occludin (fig. S1c), and low paracellular permeability (fig. S1d) comparable to previously published data[21,22].

Endothelial cell plating: For translocation experiments, cells were grown on polyester Transwell filters (3.0µm pore diameter, 0.33cm^2 surface area, Millipore, UK) coated with collagen/fibronectin in full

EBM. Once cells reached ~90% confluence, medium was changed to EBM without VEGF (hereafter termed NV-EMB), and cultured for a further 3 days. For experiments not requiring transwells, cells were plated directly onto collagen/fibronectin-coated 12 well-plates (for AuNF quantification, see below) or glass cover-slips (for AuNF visualization, see below) and grown as above.

Microglial cells: Microglia experiments were carried out on the immortalized mouse microglia N9 cell line[23], which reliably replicates primary microglia with respect to NO production, cytokine synthesis and expression of cell surface markers[24-26]. N9 microglia were cultured in Dulbecco's Modified Eagle's Medium (DMEM) with 5% FCS, 8mM L-glutamine and 50U/mL penicillin and 50µg/mL streptomycin (full DMEM).

Microglial cells were plated in 12-well plates (AuNF quantification, see below), or onto glass coverslips in 24-well plates (AuNF visualization, see below) and incubated for 24hr before experimentation began.

Cell treatment: AuNF treatments were carried out at 10 µg/mL for all nanoparticle functionalizations. At the designated time-point, medium was collected and cells thoroughly washed with HBSS to remove non-internalized AuNF. For AuNF internalization quantification, cells were collected through trypsinization (endothelial cells) or scraping (microglia) and the cell pellet digested in *aqua regia* (see below). For visualization of AuNF internalization by confocal or light-transmission microscopy, cells were washed as above before fixation with 4% PFa. Fixed cells were washed and stored at 4 ^{o}C before staining (see below).

For transcytosis experiments, AuNF were administered into the apical chamber. The basal chamber medium was then directly collected for digestion (see below) following a 6hr, 24hr or 48hr incubation. A 48hr time-point was adopted to minimize the hindrance of the transwell filter to AuNF translocation (fig. S2). Monolayer permeability was assessed through quantification of paracellular transport of FITC-dextran (4 kDa or 70 kDa) by quantifying fluorescence intensity in the basal medium (490 em/525 ex, Promega GloMax plate reader). Permeability coefficient was calculated by correcting for 4kDa FITC-dextran transport across empty transwell filters as previously described[19].

AuNF quantification

AuNF content was measured by quantifying gold concentration through either ICP-AES or ICP-MS. Cells or culture medium were digested with *aqua regia* ($HCl:HNO_3$ at 3:1) overnight and neutralized with MilliQ water before ICP-AES gold quantification. Ion counts were converted to gold mass with a gold solution standard curve. In order to control for unintended differences in the initial AuNF treatment dose, a sample of the AuNF treatment solution was analysed in parallel and the AuNF quantity in the samples expressed as a percentage of the initial dose.

Confocal microscopy

Intracellular AuNF were imaged with a laser scanning Leica SP5 confocal microscope employing an argon 546nm laser on reflectance mode. To visualize the location of endothelial cells (in confluent monolayers), nuclei were stained with DAPI and the DAPI signalled overlaid on the reflectance image. Given that microglia did not form a monolayer, their cell bodies were in addition stained with an anti-β-actin antibody to delineate their cell bodies. In order to corroborate the intracellular localization of AuNF, Z-stack series were created to visualize AuNF at different levels within the cells.

Western blotting

LAT-1 expression was verified through immunostaining of Western blots (WB) from hCMEC/D3, 1°EC, and N9 cell lysates. Cells were lysed with RIPA buffer with 10% protein inhibitors. Proteins were resolved by SDS-PAGE (10% gel) and transferred to PVDF membranes. Membranes were stained with anti-LAT1 (ThermoFisher Scientific, UK) and horse radish peroxidase (HRP)-anti-goat secondary antibody. Immunodetection was visualized through enhanced chemiluminescence (ThermoFisher Scientific, UK).

Griess assay

The Griess assay indirectly quantifies the amount of nitric oxide detecting its stable metabolite, nitrite[27]. Following treatment of microglia with AuNF or lipopolysaccharide (LPS), Griess reagent was mixed with cell culture medium in a 1:1 ratio and color development monitored by measuring optical density (OD) at 540nm (GloMax plate reader, Promega). The OD measurement was converted to concentration of nitrite with a sodium nitrite standard curve.

Cytotoxicity assays

Cytotoxicity was assessed by an MTS assay (Promega, U.K.) or an LDH release assay (Promega, U.K.). MTS assays were carried out by incubating cells with MTS reagent followed by quantification of OD at 490nm. Viability was determined as a percentage of the OD from control cells.

LDH assays were carried out by mixing cell culture medium with LDH assay reagent and LDH concentration (released LDH) quantified through OD measurement at 490 nm. Cells were then lysed in the original medium and the new LDH concentration in the culture medium (total LDH) quantified as before. Cytotoxicity was assessed by changes in the released LDH: total LDH ratio and expressed either as an absolute ratio or percentage of control treatment.

High resolution (HR)-TEM preparation and imaging

Primary brain endothelial cell monolayers grown on transwell filters were prepared for HR-TEM imaging following AuNF treatment. Monolayers were washed with 0.9% saline and fixed with 4% glutaraldehyde with 0.1% hydrogen peroxide in 0.1M HEPES buffer. Following replacement of glutaraldehyde with pure 0.1M HEPES buffer, monolayers were osmium stained by immersing in 1% OsO_4 (in 0.1M HEPES with 1.5% potassium ferricyanide, 1.5% calcium chloride) at RT. Following thorough washing with distilled water, the samples were serially dehydrated in ethanol (70%, 95%, 100%) and acetonitrile (100%). The transwell supports were then embedded in resin (35.2% Quetol, 45.5% NSA, 19.4% MNA v/v%) by serially immersing in resin:acetonitrile solution (50:50, 75:25, 100:0, 24hrs/step). The samples were then immersed in 100% resin with BDMA under vacuum and incubated at 60^{o}C for 24hrs. Once embedded, 70-100nm TEM sections were cut using a diamond knife (Diatome, Austria) on an ultramicrotome (Ultracut Reichert, Austria) and collected on copper grids. Cells were imaged using bright field TEM conditions on an FEI Titan 80-300 (Thermo Fisher Scientific, Oregon, USA) operated at 300kV.

Statistics

Results are expressed as mean$\pm$SEM of n=3, unless stated otherwise. Lines of best fit were calculated through linear regression analysis using GraphPad Prism 4.0 (GraphPad, USA). Statistics were

performed using GraphPad Prism 4.0. Statistically significant differences ($p<0.05$) were identified by Student's *t*-test (between two groups) or one-way analysis of variance (ANOVA) with Tukey's *post-hoc* (three or more groups).

Results

Functionalization of AuNF with L- or D-DOPA ligands reduces their accumulation within brain endothelial monolayers

To examine whether L/D-DOPA functionalization promotes AuNF internalization into brain endothelial cells, hCMEC/D3 human brain endothelial monolayers were treated with AuNF functionalized with the LAT-1-targeting ligands L-DOPA or D-DOPA, or the non-targeting ligands, 4-ethylcatechol (4-EC-AuNF) or dopamine (DA-AuNF). As reported previously[10], all functionalized AuNFs were approximately 90nm in diameter (by TEM) with similar surface charge, and possessed homogenous nano-flower morphology and monodispersity, hence enabling a valid comparison of biological effects. A time-course study was first carried out by treating the hCMEC/D3 monolayers with each type of functionalized AuNF for 4hr, 8hr, 12hr and 24hr. hCMEC/D3 monolayers steadily internalized 4-EC- and DA-AuNF throughout the 24hr time-course, with an average internalization rate of 2.75% and 2.72% of the initial dose (%ID)/hr, respectively (fig. 1a), reaching a maximum internalization amount of 60.4 $\pm$ 3.2 and 62.8 $\pm$ 4.7 %ID, respectively, at 24hr (fig. 1b). The increase in 4-EC- and DA-AuNF internalization by the hCMEC/D3 monolayer was accompanied by a decrease of non-internalized 4-EC- and DA-AuNF remaining in the culture medium after a 24hr incubation (3.3 $\pm$ 0.4 and 4.5 $\pm$ 0.6 %ID, respectively) (fig. 1c). Interestingly, cellular internalization of L-DOPA- and D-DOPA-AuNF was significantly lower than the 4-EC/DA-AuNF, with an internalization rate of 0.22 and 0.56 %ID/hr, respectively (fig. 1a), reaching a maximum internalization amount of 5.9 $\pm$ 1.1 and 13.0 $\pm$ 2.2 %ID, respectively, at 24hr (fig. 1b). Importantly, the low amount of internalization of the L- and D-DOPA-AuNF was accompanied by an elevated level of AuNF remaining in the cell culture medium (89.0 $\pm$ 1.8 and 77.7 $\pm$ 2.4 %ID, respectively) (fig. 1c), indicating that the low intracellular reading was

not due to either lack of available nanomaterial in the medium or loss of intracellular nanomaterial during the collection process (the lack of 100%ID recovery level, however could be due to AuNF remaining bound to the culture plate or lost during the thorough washing steps). In order to examine whether the AuNF internalization pattern was specific for the immortalized hCMEC/D3 cell line, primary rat brain endothelial monolayers (1^{o}EC) were also treated with 4-EC-, DA- or L-DOPA-AuNF. Similar to the hCMEC/D3 monolayers, the internalization rates into 1^{o}EC monolayers were comparable between the 4-EC- and DA-AuNF (1.7 and 1.8 %ID/hr, respectively). Furthermore, the pattern of higher internalization compared to L-DOPA-AuNF (0.7 %ID/hr), was maintained (fig. 1d). At 24hr, the 4-EC- and DA-AuNF had comparably high levels of internalization (40.2 $\pm$ 1.9 and 45.3 $\pm$ 5 %ID, respectively), and the lowest amount of internalisation was measured for the L-DOPA-AuNF (20.9 $\pm$ 0.5 %ID), (fig. 1e).

To verify that the AuNF associated with the hCMEC/D3 monolayers were internalized into the cells, and not simply strongly adhered to the cell membrane, the intracellular localization of the AuNFs was determined through confocal reflectance microscopy. Z-stacks spanning 4.2-7.6μm (comprising the majority of the cell height) were created for untreated and AuNF treated (4-EC- and L-DOPA-AuNF) cell monolayers (fig. 2). Although the L-DOPA-AuNF treated monolayers had a negligible AuNF signal comparable to the untreated monolayers, numerous 4-EC-AuNF inclusions were detected spanning the entire Z-stack, indicating 4-EC-AuNFs were present throughout the intracellular space, confirming cellular internalization. In addition, the AuNF localization was either restricted to the cytoplasm or lining the peri-nuclear space, with no significant penetration into the nucleus (fig. S3).

To confirm that the L-DOPA-AuNF endothelial accumulation was due to an energy-dependent, endocytic mechanism, monolayers were treated under energy-depleting conditions (4^{o}C). Incubating hCMEC/D3 monolayers (fig. S4a) or 1^{o}EC monolayers (fig. S4b) at 4^{o}C led to a significant reduction in L-DOPA-AuNF internalization compared to incubation at 37^{o}C (0.7 $\pm$ 0.3 *vs.* 2.4 $\pm$ 0.3 %ID, hCMEC/D3; -0.2 $\pm$ 0.2 *vs.* 4.7 $\pm$ 0.5 %ID, 1^{o}EC), indicating requirement of an energy-dependent endocytic process for L-DOPA-AuNF internalization in both cell types.

Functionalization of AuNF with L- or D-DOPA ligands increases their transport across brain endothelial monolayers

Given that cellular uptake does not necessarily correlate with BBB penetration[4], we hypothesized the high uptake of non-targeted AuNF may be due to intracellular sequestration, while the L/D-DOPA-functionalized AuNF may be more efficiently exocytosed as a mechanism for BBB transportation. To test this hypothesis, endothelial monolayers plated on transwell supports were treated with AuNF for 48hr and gold content in the basal chamber quantified through ICP-AES. A significantly greater amount of L-DOPA-AuNF was measured in the basolateral medium compared to the 4-EC-AuNF in both hCMEC/D3 monolayers (25.5 $\pm$ 3.0 *vs.* 16.9 $\pm$ 0.99 %ID) (fig. 3a) and primary rat brain endothelial monolayers (58.6 $\pm$ 7.4 *vs.* 35.6 $\pm$ 1.1 %ID) (fig. 3b). Importantly, treatment with either L-DOPA- or 4-EC-AuNF did not induce cytotoxicity (fig. S5a) or increase permeability of either the hCMEC/D3 monolayers (fig. S5b) or the 1^{o}EC monolayers (fig. S5c), indicating the increase in basolateral AuNF concentration was not due to a breakdown in monolayer integrity following AuNF treatment.

To confirm transport of L-DOPA-AuNF through the BBB, interaction of L-DOPA-AuNF with 1^{o}EC monolayers was visualized through HR-TEM (fig. 3c). L-DOPA-AuNF were observed in three stages of translocation: 1) in close contact with the apical cell membrane without internalization (top panel, dashed arrow); 2) properly internalized into the intracellular space (bottom panel, arrow); 3) released into the basolateral space (bottom panel, arrow head), confirming transcellular transport of the L-DOPA-AuNF.

The transport of AuNF across peripheral endothelial monolayers was examined by treating human umbilical vein endothelial cell monolayers with L-DOPA- or 4-EC-AuNF for 6hr (fig. S6a) or 24hrs (fig. S6b) and quantifying basal gold through ICP-MS. Similarly to rat brain endothelial monolayers, transport of L-DOPA-AuNF across human umbilical vein endothelial cell monolayers was higher compared to 4-EC-AuNF at both time-points. Furthermore, the rate of transport for 4-EC- and L-DOPA-AuNF was comparable to that seen in brain endothelial monolayers (0.74 and 1.15%ID/hr, respectively). The involvement of direct transport across the LAT-1 channel pore was examined by addition of increasing concentrations of the LAT-1 competitive substrate 3-iodo-L-tyrosine.

Interestingly, no effect on AuNF transport was seen for either functionalization scheme at either 6hr (fig. S6c) or 24 hr (fig. S6d). Importantly, the permeability of the endothelial monolayer was not affected (24hrs) by either AuNF treatment or 3-iodo-L-tyrosine co-treatment (fig. S6d).

Brain macrophages (microglia) efficiently internalize AuNF functionalized with L- or D-DOPA ligands without induction of inflammation

Brain macrophages (microglia) are the main cell type responsible for clearance of foreign entities, and capture and process exogenous nanomaterials[28, 29]. Therefore, to examine the capacity of AuNF to be cleared from the brain following BBB penetration, internalization of AuNF into microglia was quantified. Interestingly, a 24hr treatment with AuNF led to a reversed pattern of internalization compared to internalization into endothelial monolayers, with a higher intracellular concentration for the L-DOPA- and D-DOPA-AuNF (37.9 $\pm$ 2.3 and 41.9 $\pm$ 5.9 %ID) compared to the 4-EC- and DA-AuNF (fig. 4a). Importantly, the amount of AuNF internalization was inversely proportional to the amount of non-internalized AuNF remaining in the culture medium (fig. 4b). This pattern of internalization was also evident at 8hr post-treatment (fig. S7a,b). Furthermore, L-DOPA-AuNF internalization was significantly inhibited by incubation at 4^{o}C, indicating an energy-dependent process (fig. 4c). While there was no effect of low temperature incubation on internalization of 4-EC-AuNF (fig. 4c), this effect could be due to the short incubation time (4hr) and low internalization rate, or an energy independent process mediated by the AuNF morphology. In order to determine whether AuNF internalization induced inflammation, microglia cells were treated with L-DOPA- or DA-AuNF for 24hr, followed by quantification of nitric oxide (NO) production. Neither AuNF increased NO production comparted to non-treated cells (fig. 4d). In contrast, treatment with LPS induced a marked increase in NO production, demonstrating the ability of the cells to become inflamed (fig. 5d).

Light transmission microscopy and confocal reflectance microscopy analysis of microglia cells treated with 4-EC- or L-DOPA-AuNF echoed the ICP-AES results, with comparably low AuNF detection levels under light microscopy between untreated and 4-EC-AuNF treated cells (fig. 5 a,b), and a

marginally increased gold detection level in 4-EC-AuNF treated cells compared to untreated cells under confocal reflectance microscopy (fig. 5 d, e). Conversely, a significantly stronger AuNF detection signal for the L-DOPA-AuNF treated cells was seen under both light microscopy (fig. 5c) and confocal reflectance microscopy (fig. 5f). Z-stack analysis revealed L-DOPA-AuNF could be detected throughout the cell (fig. S8), indicating proper cellular internalization. In addition, the Z-stack analysis revealed AuNF internalization was restricted to the cytoplasmic space surrounding the nucleus similarly to endothelial cells.

Expression of LAT-1 was confirmed through Western blot (fig. S9). A specific protein band of 55kDa, corresponding to the molecular weight of LAT-1, was detected for all three cell types, demonstrating positive LAT-1 expression, as has been shown for macrophages and brain endothelial cells[30-32].

Discussion

Our results demonstrate that AuNF functionalization with L-DOPA or D-DOPA ligands leads to significantly higher AuNF transportation across an *in vitro* BBB model formed by a hCMEC/D3 monolayer. Interestingly, efficient BBB transcytosis occurred with minimal cellular accumulation, suggesting efficient endothelial escape. In contrast, AuNFs functionalized with the non-targeting control ligand, 4-EC, had lower rates of BBB transcytosis but significantly higher cellular accumulation, indicating sequestration by the endothelial cells. Importantly, the uptake and transport trend in immortalized human brain endothelial cells was maintained in experiments employing isolated primary rat brain endothelial cells, excluding the possibility of an experimental artefact due to the immortalization process. In addition, confocal reflectance imaging and transmission electron microscopy studies, coupled with the low-temperature inhibition assays, demonstrated that the majority of cell-associated AuNF were internalized in an energy-dependent process. Crucially, the amount of L-DOPA-AuNFs transported across the BBB (1.22%ID/hr) is higher than what has been reported in the literature for *in vitro* BBB models (0.1-1%ID/hr)[5, 33-35]. Furthermore, the transportation rate of AuNF across the BBB monolayer was comparable to that seen in monolayers composed of peripheral human

umbilical vein endothelial cells, indicating L-DOPA-AuNF are indeed able to overcome the impermeability of the BBB. Hence, functionalization of AuNF with L-DOPA confers a significantly improved strategy for the highly efficient shuttling of nanoparticles into the brain.

Significantly, a reversed trend of AuNP uptake was seen in microglia cells, with the highest accumulation occurring for the L-DOPA/D-DOPA functionalized AuNF. Again, light microscopy and confocal reflectance microscopy, coupled with uptake assays at low temperature, indicated L-DOPA-AuNF uptake was indeed intracellular. The discrepancy in AuNF uptake between cell types may be due to differences in membrane dynamics governing the endocytosis of the target receptor (presumably LAT-1) in each phenotype. Cellular internalization of free L-DOPA through the LAT-1 channel pore occurs independently of LAT-1 endocytosis[36, 37]. However, as the size of the AuNF used in this study is significantly larger than the size of the LAT-1 transporter[38], AuNF uptake must occur through an alternative, endocytosis-dependent mechanism, possibly driven through target protein clustering at the cell membrane due to the multi-valent L-DOPA functionalization of AuNF, as has been shown for multimeric antibodies inducing clustering and internalization of membrane proteins on endothelial cells[39]. In support of this hypothesis, co-treatment with 3-iodo-L-tyrosine, a competitive ligand for direct transport across the LAT-1 channel pore, did not affect the transport of L-DOPA-AuNF across endothelial monolayers. Hence, LAT-1 membrane clustering in brain endothelial cells might lead to an association with guiding proteins responsible for transport of the AuNF across the monolayer, resulting in exocytosis at the basolateral membrane. Conversely, in macrophages, which have been shown to express LAT-1[30,31] but do not form monolayers, the internalization mechanism might not be equipped with signals to promote cargo transcytosis, leading to capture of the AuNF within the cell body. However, as microglia are phagocytic cells, a receptor independent internalization mechanism may also significantly contribute to AuNF capture.

In addition to cellular phenotype, the geometry of the AuNF may also modulate the uptake of the nanomaterials into brain endothelial cells. In a study on the uptake of negatively charged, hydrophilic, polyethylene glycol (PEG)-NPs of varying aspect-ratios, it was reported that epithelial cells preferentially internalized disk-shaped PEG-NPs compared to rod-like and smaller disk-like PEG

NPs[40]. Hence, it is possible that the spikes of the present AuNF modulate cell interaction to induce endocytic entry across the plasma membrane of the brain endothelial cells. The spikes of the AuNFs may also be able to translocate across the plasma membrane of the brain endothelial cells, which may promote subsequent transport of the AuNFs across the BBB: the TEM images in figure 4 show very intimate contact between the spikes of the AuNF and are suggestive of this process. Indeed, such a mechanism has been proposed previously to facilitate transport of high aspect-ratio carbon nanotubes across brain endothelial cells[41]. Future work will deconvolute the effects of geometry and surface functionalisation on cellular internalization.

Importantly, the present work shows that even though L-DOPA-AuNF are highly internalized by microglial cells, this does not induce microglial activation, indicating detrimental brain inflammation will not occur following L-DOPA-AuNF brain entry. In addition, given that microglia are able to internalize nanomaterials without inducing overt inflammation[29], the present work indicates L-DOPA-AuNF will be promptly and safely cleared from the extracellular space following brain delivery of their pay-load, further supporting the safe application of these nanoparticles as brain-delivery nano-vehicles vehicles in the clinic. Furthermore, confocal microscopy indicated that internalized AuNF remained in the cytoplasmic area or lined the nuclear barrier without causing damage to the nucleus. This observation further underlines the biosafety of the present AuNF-based nano-vehicle formulation, as previous studies have shown that treatment with gold nanoparticles of similar size leads to nuclear localization and cytoxicity[42].

In conclusion, we show that the L-DOPA-functionalized AuNFs are efficiently transported across well-established *in vitro* BBB models in a ligand-dependent manner and are readily taken up by brain macrophages with no obvious inflammatory effects. These findings lay the foundations for a gold theranostic nano-vehicle with significantly higher access to the brain than previously possible, and with minimal cytotoxicity and inflammatory responses in the brain following payload delivery.

Abbreviations

L/D-DOPA, L/D-3,4-dihydroxyphenyalanine; DA, dopamine; 4-EC, 4-ethyl-catecholamine; BBB, blood-brain barrier; AuNF, gold nanoflower; LAT-1, large neutral amino acid transporter-1; hCMEC/D3, human cerebral microvascular endothelial cell/D3 clone

References

1. Preston JE, Abbott JN, Begley DJ. Transcytosis of macromolecules at the blood-brain barrier. *Adv Pharmacol* 2014; **71**:147-163.
2. Alkilany A, Murphy C. Toxicity and cellular uptake of gold nanoparticles: what we have learned so far? *J Nanopart Res* 2010; **12** (7): 2313-2333.
3. Popovtzer R, Agrawal A, Kotov N, Popovtzer A, Balter J, Carey TE et al. Targeted gold nanoparticles enable molecular CT imaging of cancer. *Nano Lett* 2008; **8** (12):4593-4596.
4. Wiley DT, Webster P, Gale A, Davis, ME. Transcytosis and brain uptake of transferrin-containing nanoparticles by tuning avidity to transferrin receptor. *Proc Natl Acad Sci U S A* 2013; **110** (21): 8662-7.
5. Clark AJ, Davis ME. Increased brain uptake of targeted nanoparticles by adding an acid-cleavable linkage between transferrin and the nanoparticle core. *Proc Natl Acad Sci U S A* 2015; **112** (40): 12486-91.
6. Gromnicova R, Davies HA, Sreekanthreddy P, Romero IA, Lund T, Roitt IM et al. Glucose-coated gold nanoparticles transfer across human brain endothelium and enter astrocytes in vitro. *PLoS One* 2013; **8** (12): e81043.
7. Shilo M, Motiei M, Hana P, Popovtzer R. Transport of nanoparticles through the blood-brain barrier for imaging and therapeutic applications. *Nanoscale* 2014; **6** (4): 2146-52.

8. Boado RJ, Li JY, Nagaya M, Zhang C, Pardridge WM. Selective expression of the large neutral amino acid transporter at the blood-brain barrier. *Proc Natl Acad Sci U S A* 1999; **96** (21): 12079-84.

9. Dickens D, Chiduza G, Wright G, Pirmohamed M, Antonyuk S, Hasnain S. Modulation of LAT1 (SLC7A5) transporter activity and stability by membrane cholesterol. *Sci Rep* 2017; **7**: 43580.

10. Ong ZY, Chen S, Nabavi E, Regoutz A, Payne DJ, Elson DS, Dexter DT, Dunlop IE, Porter AE. Multibranched Gold Nanoparticles with Intrinsic LAT-1 Targeting Capabilities for Selective Photothermal Therapy of Breast Cancer. *ACS Appl Mater Interfaces* 2017; **9** (45): 39259-39270.

11. Yanagida O, Kanai Y, Chairoungdua A, Kim DK, Segawa H, Nii T et al. Human L-type amino acid tranporter 1 (LAT1): characterization of function and expression in tumor cell lines. *Biochim Biophys Acta* 2001; **1514 (**2): 291-302.

12. Silk JD, Lakhal S, Laynes R, Vallius L, Karydis I, Marcea C et al. Indoleamine 2,3-dioxygenase induces expression of a novel tryptophan transporter in mouse and human tumor cells. *J Immunol* 2011; **187** (4): 1617-1625.

13. Pinho MJ, Serrao MP, Gomes P, Hopfer U, Jose PA, Soares-da-Silva P. Over-expression of renal LAT1 and LAT2 and enhanced L-DOPA uptake in SHR immortalized renal proximal tubular cells. *Kidney Int* 2004; **66** (1): 216-26.

14. Weksler B, Romero IA, Couraud PO. The hCMEC/D3 cell line as a model of the human blood brain barrier. *Fluids Barriers CNS* 2013; **10** (16): 1-10.

15. Uchino H, Kanai Y, Kim DK, Wempe MF, Chairoungdua A, Morimoto E, et al. Transport of amino acid-related compounds mediated by L-type amino acid transporter 1 (LAT1): insights into the mechanisms of substrate recognition. *Mol Pharmacol* 2002; **61** (4): 729-37.

16. Weksler BB, Subileau EA, Perrière N, Charneau P, Holloway K, Leveque M, et al. Blood-brain barrier-specific properties of a human adult brain endothelial cell line. *FASEB J* 2005; **19** (13): 1872-4.

17. Laakkonen JP, Engler T, Romero IA, Weksler B, Couraud PO, Kreppel F, et al.Transcellular targeting of fiber- and hexon-modified adenovirus vectors across the brain microvascular endothelial cells in vitro. *PloS One* 2012; **7** (9): e45977.

18. Tai LM, Reddy PS, Lopez-Ramirez MA, Davies HA, Male DK, Loughlin AJ, et al. Polarized P-glycoprotein expression by the immortalised human brain endothelial cell line, hCMEC/D3, restricts apical-to-basolateral permeability to rhodamine 123. *Brain Res* 2009; **1292**: 14-24.

19. Gonzalez-Carter D, Goode AE, Fiammengo R, Dunlop IE, Dexter DT, Porter AE. Inhibition of leptin-ObR interaction does not prevent leptin translocation across a human blood-brain barrier model. *J Neuroendocrinol* 2016; **28** (6): 12.

20. Watson P, Paterson J, Thom G, Ginman U, Lundquist S, Webster C. Modelling the endothelial blood-CNS barriers: a method for the production of robust in vitro models of the rat blood-brain barrier and blood-spinal cord barrier. *BMC Neurosci* 2013; **14**: 59.

21. Gaillard P, de Boer A. Relationship between permeability status of the blood-brain barrier and in vitro permeability coefficient of a drug. *Eur J Pharm Sci* 2000; **12** (2): 95-102.
22. Steiner O, Coisne C, Engelhardt B, Lyck R. Comparison of immortalized bEnd5 and primary mouse brain microvascular endothelial cells as in vitro blood-brain barrier models for the study of T cell extravasation. *J Cereb Blood FLow Metab* 2011; **31** (1): 315-327.
23. Righi M, Mori L, De Libero G, Sironi M, Biondi A, Mantovani A, et al. Monokine production by microglial cell clones. *Eur J Immunol* 1989; **19** (8): 1443-8.
24. Bulgarelli I, Tamiazzo L, Bresciani E, Rapetti D, Caporali S, Lattuada D, et al. Desacyl-ghrelin and synthetic GH-secretagogues modulate the production of inflammatory cytokines in mouse microglia cells stimulated by beta-amyloid fibrils. *J Neurosci Res* 2009; **87** (12): 2718-27.
25. Bureau G, Longpre F, Martinoli MG. Resveratrol and quercetin, two natural polyphenols, reduce apoptotic neuronal cell death induced by neuroinflammation. *J Neurosci Res* 2008; **86** (2): 403-10.
26. Chang LC, Tsao LT, Chang CS, Chen CJ, Huang LJ, Kuo SC, et al. Inhibition of nitric oxide production by the carbazole compound LCY-2-CHO via blockade of activator protein-1 and CCAAT/enhancer-binding protein activation in microglia. *Biochem Pharmacol* 2008;**76** (4): 507-19.
27. Giustarini D, Rossi R, Milzani A, Dalle-Donne I. Nitrite and nitrate measurement by Griess reagent in human plasma: evaluation of interferences and standardization. *Methods Enzymol* 2008; **440**: 361-80.
28. Gonzalez-Carter DA, Leo BF, Ruenraroengsak P, Chen S, Goode AE, Theodorou IG, Chung KF, Carzaniga R, Shaffer MS, Dexter DT, Ryan MP, Porter AE. Silver nanoparticles reduce brain inflammation and related neurotoxicity through induction of H_2S-synthesizing enzymes. *Sci Rep* 2017; **7**: 42871.
29. Goode AE, Gonzalez-Carter DA, Motskin M, Pienaar I, Chen S, Hu S, Ruenraroengsak P, Ryan MP, Shaffer MS, Dexter DT, Porter AE. High resolution and dynamic imaging of biopersistence and bioreactivity of extra and intracellular MWNTs exposed to microglial cells. *Biomaterials* 2015; **70**: 57-70.
30. Martinez F, Gordon S, Locati M, Mantovani A. Transcriptional profiling of the human monocyte-to-macrophage differentiation and polarization: new molecules and patterns of gene expression. *J Immunol* 2006; **177** (10): 7303-7311.
31. Brahmajothi MV, Sun NZ, Auten RL. S-nitrosothiol transport via PEPT2 mediates biological effects of nitric oxide gas exposure in macrophages. *Am J Respir Cell Mol Biol* 2013; **48** (2): 230-9.
32. Daneman R, Zhou L, Agalliu D, Cahoy JD, Kaushal A, Barres BA. The mouse blood-brain barrier transcriptome: a new resource for understanding the development and function of brain endothelial cells. *PLoS One* 2010; **5** (10): e13741.

33. Ruff J, Hüwel S, Kogan MJ, Simon U, Galla HJ. The effects of gold nanoparticles functionalized with ß-amyloid specific peptides on an in vitro model of blood-brain barrier. *Nanomedicine* 2017; **13** (5): 1645-1652.

34. Falanga AP, Pitingolo G, Celentano M, Cosentino A, Melone P, Vecchione R, et al. Shuttle-mediated nanoparticle transport across an in vitro brain endothelium under flow conditions. *Biotechnol Bioeng* 2017; **114** (5): 1087-1095.

35. Georgieva JV, Kalicharan D, Couraud PO, Romero IA, Weksler B, Hoekstra D, et al. Surface characteristics of nanoparticles determine their intracellular fate in and processing by human blood-brain barrier endothelial cells in vitro. *Mol Ther* 2011; **19** (2): 318-25.

36. del Amo EM, Urtti A, Yliperttula M. Pharmacokinetic role of L-type amino acid transporters LAT1 and LAT2. *Eur J Pharm Sci* 2008; **35** (3): 161-74.

37. Meier C, Ristic Z, Klauser S, Verrey F. Activation of system L heterodimeric amino acid exchangers by intracellular substrates. *EMBO J* 2002; **21** (4): 580-9.

38. Napolitano L, Scalise M, Galluccio M, Pochini L, Albanese LM, Indiveri C. LAT1 is the transport competent unit of the LAT1/CD98 heterodimeric amino acid transporter. *Int J Biochem Cell Biol* 2015; **67**: 25-33.

39. Muro S, Wiewrodt R, Thomas A, Koniaris L, Albelda SM, Muzykantov VR, et al. A novel endocytic pathway induced by clustering endothelial ICAM-1 or PECAM-1. *J Cell Sci* 2003; **116** (8): 1599-609.

40. Agarwal R, Singh V, Jurney P, Shi L, Sreenivasan SV, Roy K. Mammalian cells preferentially internalize hydrogel nanodiscs over nanorods and use shape-specific uptake mechanisms. *Proc Natl Acad Sci U S A* 2013; **110** (43): 17247-52.

41. Kafa H, Wang JT, Rubio N, Venner K, Anderson G, Pach E, Ballesteros B, Preston JE, Abbott NJ, Al-Jamal KT. The interaction of carbon nanotubes with an in vitro blood-brain barrier model and mouse brain in vivo. *Biomaterials* 2015; **53**: 437-52.

42. Kodiha M, Hutter E, Boridy S, Juhas M, Maysinger D, Stochaj U. Gold nanoparticles induce nuclear damage in breast cancer cells, which is further amplified by hyperthermia. *Cell Mol Life Sci* 2014; **71** (21); 4259-73.

Figure legends

Figure 1. Internalization of gold nanoflowers (AuNF) into hCMEC/D3 or primary brain endothelial cell (1°EC) monolayers. hCMEC/D3 or 1°EC monolayers were treated with 10µg/mL AuNF functionalized with either 4-ethylcatechol (4-EC), dopamine (DA), L-DOPA or D-DOPA. AuNF internalization rate in hCMEC/D3 (a) or 1°EC (d) was calculated by quantifying cell-associated gold through ICP-AES at 4, 8, 12 and 24hr following treatment. The total amount of internalized AuNF into hCMEC/D3 (b) or 1°EC (e), as well as AuNF remaining in the culture medium of hCMEC/D3 (c), following a 24hr incubation was similarly measured. AuNF quantity was calculated as a percentage of the initial dose (%ID). Results are displayed as mean±SEM of at least three independent experiments. *,*** denote $p<0.05$ and 0.001, respectively *vs.* 4-EC. ##,### denote $p<0.005$, 0.001, respectively *vs.* DA. Statistical significance was determined by a one-way ANOVA with Tukey's *post-hoc* test.

Figure 2. Confocal reflectance microscopy Z-stack imaging of intracellular gold nanoflowers (AuNF) in hCMEC/D3 human endothelial monolayers. AuNF internalization into hCMEC/D3 monolayers following a 24hr treatment (10µg/mL) was visualized through confocal reflectance microscopy employing an argon 546 nm laser. The intracellular distribution of AuNF was visualized by constructing Z-stacks (of 4.2µm or 7.6µm depth) for untreated cells (top panels) or cells treated with 4-EC-AuNF (middle panels) or L-DOPA-AuNF (bottom panels). Laser power, exposure and gain

parameters were kept constant for all images. Images are representative of three independent experiments. Blue=DAPI, red=AuNF. Scale bar=25µm.

Figure 3. Transport of gold nanoflowers (AuNF) across BBB endothelial monolayers. hCMEC/D3 (a) or primary brain endothelial cell (b) monolayers grown on transwell supports were treated with AuNF (10µg/mL) functionalized with 4-ethylcatecholamine (4-EC) or L-DOPA. Following a 48hr incubation period, AuNF transport across the monolayers was quantified by measuring gold content in the basolateral cell medium (basal Au) through ICP-AES. AuNF transport was calculated as percentage of the initial dose (%ID). Transport of L-DOPA-AuNF across primary brain endothelial monolayers grown on transwell supports was visualized (24hr) through high-resolution TEM (c). Images revealed AuNF closely interacted with the apical cell membrane (top panel, dashed arrow). In addition, AuNF were internalized into the intracellular space (bottom panel, solid arrow), as well as exiting into the basolateral space (bottom panel, arrow head), demonstrating successful transcytosis of the AuNF. Results in are displayed as mean±SEM of five (a) or three (b) independent experiments. *denotes $p<0.05$ as determined by a Student's *t*-test. Images are representative of two independent monolayers.

Figure 4. Internalization of gold nanoflowers (AuNF) into brain macrophages (microglia). Microglia cells (N9 cell line) were treated with 10µg/mL AuNF functionalized with either 4-ethylcatecholamine (4-EC), dopamine (DA), L-DOPA or D-DOPA. AuNF cellular internalization (a) and AuNF remaining in the culture medium (b) 24hr following treatment were calculated by quantifying gold through ICP-AES. AuNF quantity was calculated as a percentage of the initial dose (%ID). Results are displayed as mean±SEM of at least three independent experiments. ***denotes $p<0.001$, *vs.* 4-EC. ###denotes $p<0.\ 0.001$ *vs.* DA. Statistical significance was determined by a one-way ANOVA with Tukey's *post-hoc* test.

Figure 5. Light transmission and confocal reflectance microscopy imaging of intracellular gold nanoflowers (AuNF) in brain macrophage (microglia) cells. Internalization of AuNF into microglia cells (N9 cell line) following a 24hr treatment (10µg/mL) was visualized through light transmission microscopy (a-c) and confocal reflectance imaging (d-f) employing an argon 546 nm laser. To visualize the cell bodies, microglia were stained with an anti-β-actin antibody. Laser power, exposure and gain parameters were kept constant for all images. Images are representative of three independent experiments. Blue=DAPI, red=β-actin immunofluorescence, yellow=AuNF. Scale bar=55µm (top panels) or 25µm (bottom panels).

Figures.

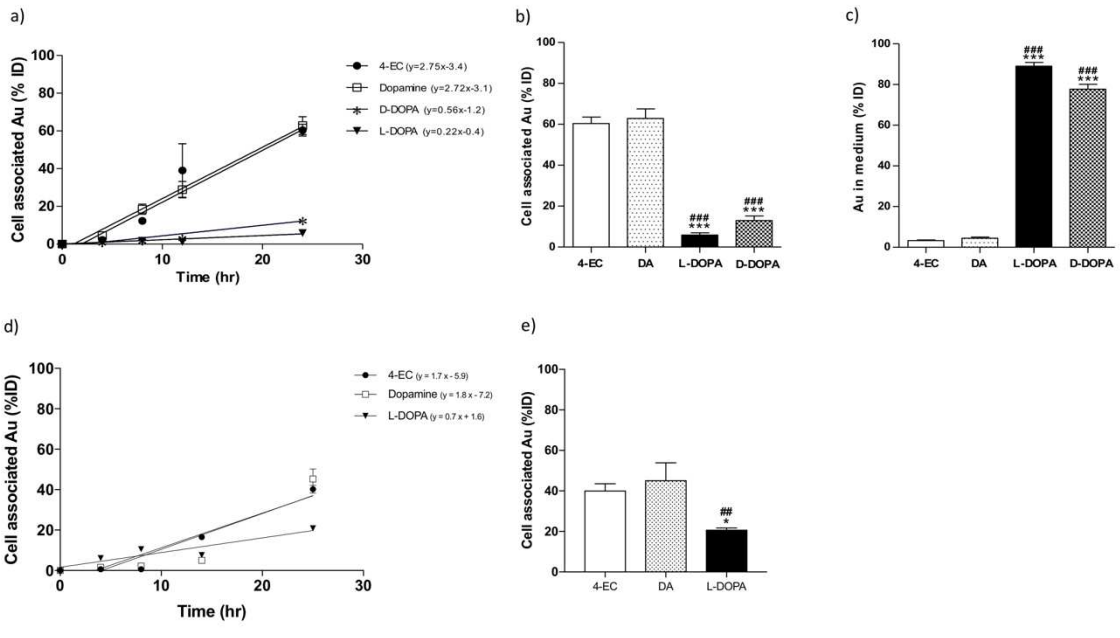
a)
Cell associated Au (% ID)
Time (hr)
4-EC (y=2.75x-3.4)
Dopamine (y=2.72x-3.1)
D-DOPA (y=0.56x-1.2)
L-DOPA (y=0.22x-0.4)
b)
Cell associated Au (% ID)
4-EC
DA
L-DOPA
D-DOPA
c)
Au in medium (% ID)
4-EC
DA
L-DOPA
D-DOPA
d)
Cell associated Au (%ID)
Time (hr)
4-EC (y = 1.7 x - 5.9)
Dopamine (y = 1.8 x - 7.2)
L-DOPA (y = 0.7 x + 1.6)
e)
Cell associated Au (%ID)
4-EC
DA
L-DOPA

Figure 1.

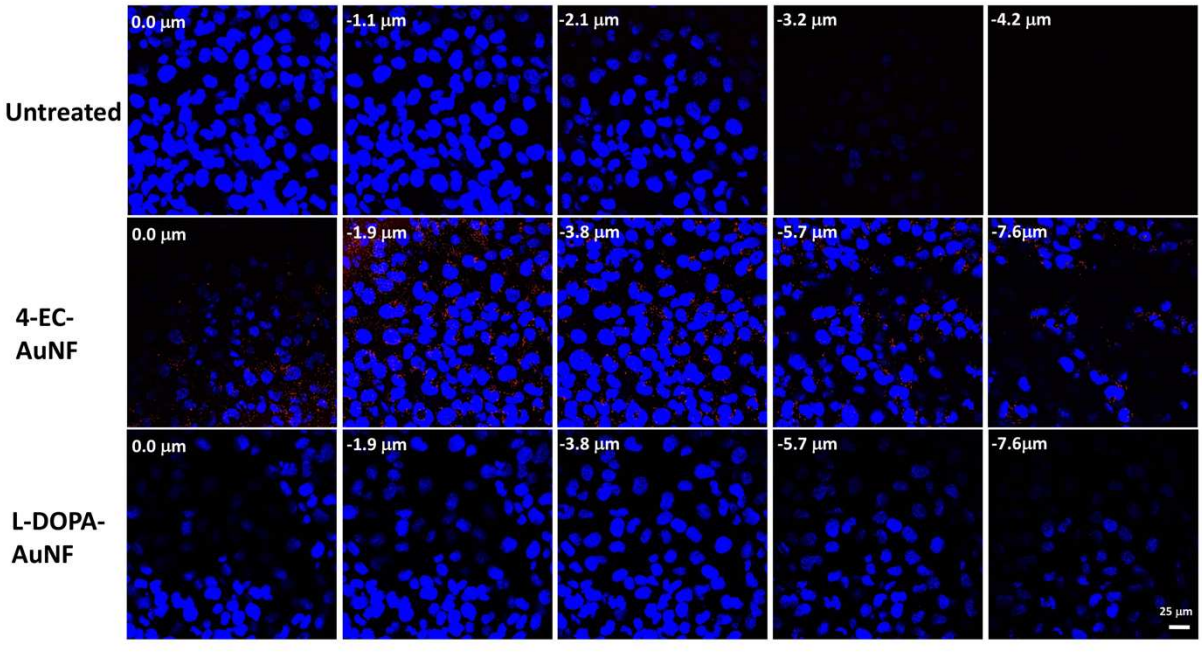
Untreated
4-EC-AuNF
L-DOPA-AuNF
0.0 µm
-1.1 µm
-2.1 µm
-3.2 µm
-4.2 µm
0.0 µm
-1.9 µm
-3.8 µm
-5.7 µm
-7.6µm
0.0 µm
-1.9 µm
-3.8 µm
-5.7 µm
-7.6µm
25 µm

Figure 2.

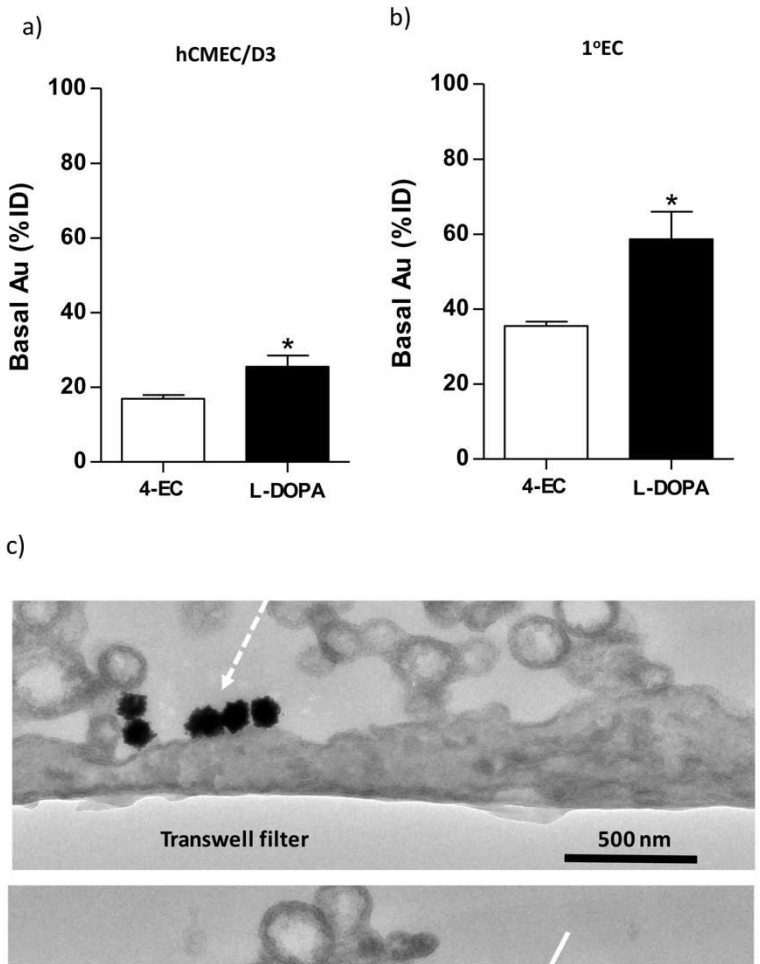
a)
hCMEC/D3
Basal Au (%ID)
100
80
60
40
20
0
*
4-EC
L-DOPA
b)
1°EC
Basal Au (%ID)
100
80
60
40
20
0
*
4-EC
L-DOPA
c)
Transwell filter
500 nm

Figure 3.

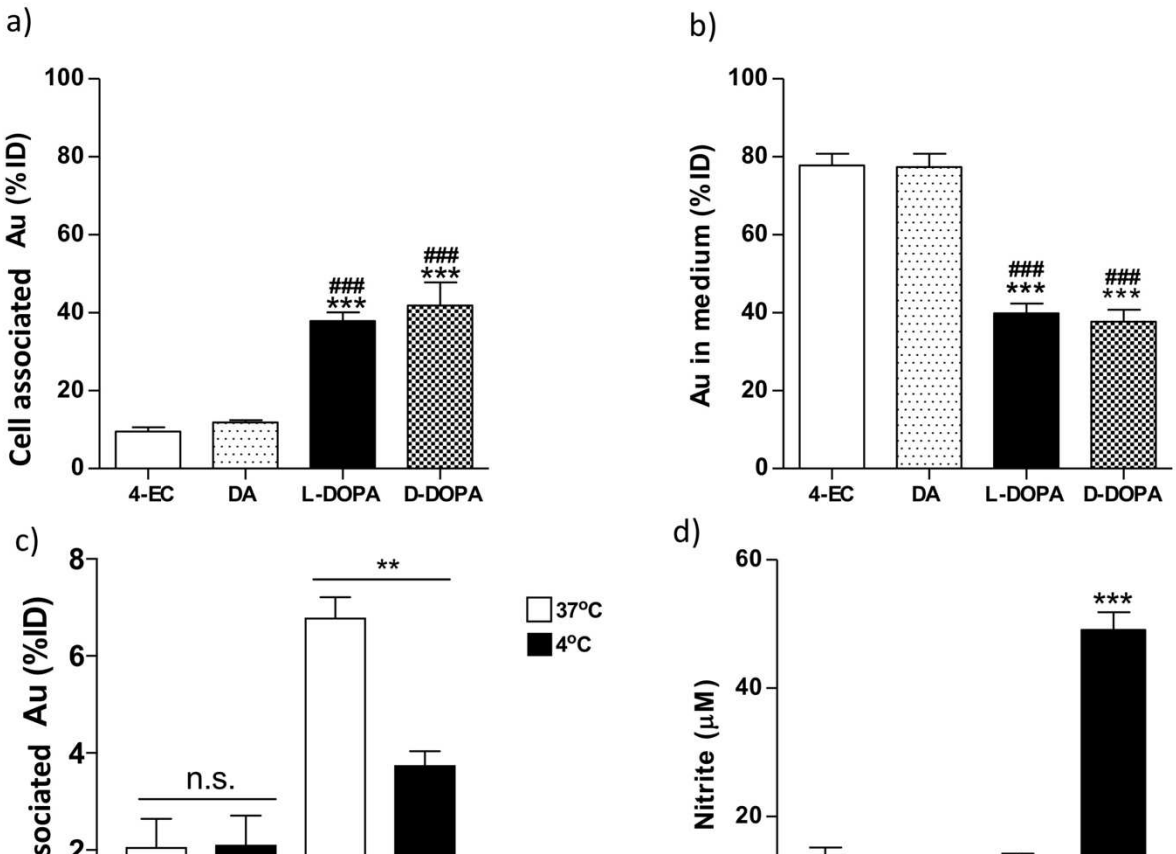
a)
Cell associated Au (%ID)
100
80
60
40
20
0
###
***
###
***
4-EC
DA
L-DOPA
D-DOPA
b)
Au in medium (%ID)
100
80
60
40
20
0
###
***
###
***
4-EC
DA
L-DOPA
D-DOPA
c)
sociated Au (%ID)
8
6
4
2
n.s.
**
37°C
4°C
d)
Nitrite (µM)
60
40
20
***

Figure 4.

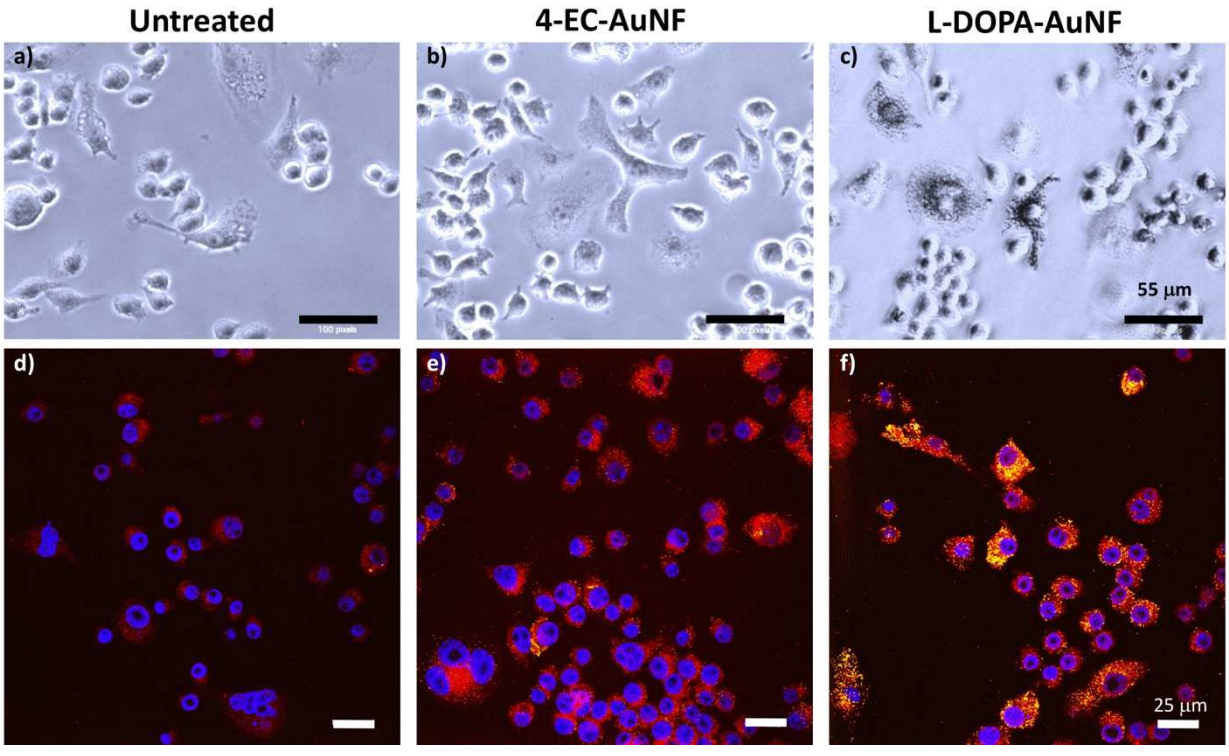

Figure 5.